










Ferroelectricity in the $1 \mu\text{C cm}^{-2}$ range induced by canted antiferromagnetism in $(\text{LaMn}_3)\text{Mn}_4\text{O}_{12}$

Cite as: Appl. Phys. Lett. **115**, 152902 (2019); <https://doi.org/10.1063/1.5108640>

Submitted: 09 May 2019 . Accepted: 09 September 2019 . Published Online: 10 October 2019

A. Gauzzi , F. P. Milton, V. Pascotto Gastaldo , M. Verseils , A. J. Gualdi , D. von Dreifus , Y. Klein , D. Garcia, A. J. A. de Oliveira , P. Bordet , and E. Gilioli 



View Online



Export Citation



CrossMark

ARTICLES YOU MAY BE INTERESTED IN

[Observing large ferroelectric polarization in top-electrode-free Al:HfO₂ thin films with Al-rich strip structures](#)

Applied Physics Letters **115**, 152901 (2019); <https://doi.org/10.1063/1.5110668>

[Laser-generated focused ultrasound transmitters with frequency-tuned outputs over sub-10-MHz range](#)

Applied Physics Letters **115**, 154103 (2019); <https://doi.org/10.1063/1.5106415>

[Terahertz sensing of 7 nm dielectric film with bound states in the continuum metasurfaces](#)

Applied Physics Letters **115**, 151105 (2019); <https://doi.org/10.1063/1.5110383>



Measure Ready
M91 FastHall™ Controller

A revolutionary new instrument for complete Hall analysis

[See the video](#)

Lake Shore
CRYOTRONICS

Ferroelectricity in the $1 \mu\text{C cm}^{-2}$ range induced by canted antiferromagnetism in $(\text{LaMn}_3)\text{Mn}_4\text{O}_{12}$

Cite as: Appl. Phys. Lett. **115**, 152902 (2019); doi: [10.1063/1.5108640](https://doi.org/10.1063/1.5108640)

Submitted: 9 May 2019 · Accepted: 9 September 2019 ·

Published Online: 10 October 2019



View Online



Export Citation



CrossMark

A. Gauzzi,^{1,a)}  F. P. Milton,² V. Pascotto Gastaldo,²  M. Verseils,¹  A. J. Gualdi,²  D. von Dreifus,²  Y. Klein,¹ 
D. Garcia,² A. J. A. de Oliveira,²  P. Bordet,³  and E. Gilioli⁴ 

AFFILIATIONS

¹IMPMC, Sorbonne Université, CNRS, MNHN, 4, place Jussieu, 75005 Paris, France

²Departamento de Física, Universidade Federal de São Carlos, Rodovia Washington Luís, km 235, São Carlos, São Paulo 13565-905, Brazil

³Institut Néel, CNRS and Université Grenoble Alpes, 38042 Grenoble, France

⁴Istituto dei Materiali per Elettronica e Magnetismo-CNR, Area delle Scienze, 43100 Parma, Italy

a) Author to whom correspondence should be addressed: andrea.gauzzi@sorbonne-universite.fr

ABSTRACT

Pyroelectric current and field-dependent specific heat measurements on polycrystalline samples of the quadruple perovskite $(\text{LaMn}_3)\text{Mn}_4\text{O}_{12}$ give evidence of ferroelectricity driven by the canted antiferromagnetic ordering of the B -site Mn^{3+} ions at $T_{N,B} = 78$ K with record large remnant electric polarization up to $0.56 \mu\text{C cm}^{-2}$. X-ray diffraction measurements indicate an anomalous behavior of the monoclinic β angle at $T_{N,B}$, which suggests that the polarization lies in the ac -plane, where the moments are collinear, and that symmetric exchange striction is the mechanism of spin-driven ferroelectricity. Polarization values up to $\sim 3\text{--}6 \mu\text{C cm}^{-2}$ are expected in single crystals or epitaxial films, which would enable the development of practical multiferroic applications.

Published under license by AIP Publishing. <https://doi.org/10.1063/1.5108640>

In the search for multiferroic materials for applications, magnetic ferroelectrics, where ferroelectricity is induced by magnetic order, are promising for their inherently strong magnetoelectric couplings.¹ The challenge is to enhance the remnant polarization, which is typically small in these materials, $P \sim 0.1 \mu\text{C cm}^{-2}$. This has been attributed to the weakness of the spin-orbit interaction in noncollinear spin structures,² where P arises from the antisymmetric exchange striction (inverse Dzyaloshinskii-Moriya interaction) between neighboring spins. More promising are collinear spin structures, where values up to $\sim 10 \mu\text{C cm}^{-2}$ are predicted due to the comparatively strong symmetric exchange striction.³ This prediction is supported by the large value $P \sim 1 \mu\text{C cm}^{-2}$ reached under pressure in the perovskitelike compound TbMnO_3 , characterized by a collinear E-structure.⁴ The symmetric exchange mechanism has been invoked to account for a remarkable P -enhancement up to $0.27 \mu\text{C cm}^{-2}$ in another manganese oxide, $(\text{CaMn}_3)\text{Mn}_4\text{O}_{12}$ (CMO),^{5,6} with a “quadruple perovskite” (QP) $AA'_3B_4\text{O}_{12}$ structure, characterized by two distinct A' and B Mn sites.⁷ However, the role of this mechanism in CMO remains controversial^{8,9} possibly because of a complex interplay of incommensurate helicoidal spin structure and charge and orbital ordering of the Mn^{3+} and Mn^{4+} ions.¹⁰

Here, we show that $(\text{LaMn}_3)\text{Mn}_4\text{O}_{12}$ (Refs. 11 and 12) (LMO) is a model system to investigate the role of symmetric exchange striction in magnetic ferroelectricity. LMO shares with CMO a similar QP structure but exhibits simpler structural and electronic properties. LMO is a single-valent Mn^{3+} system with neither charge orderings nor incommensurate structural modulations.¹¹ The $Im\bar{3}$ cubic structure stable at high temperatures undergoes a monoclinic $I2/m$ distortion at 653 K.¹² The B -site Mn^{3+} ions antiferromagnetically (AFM) order forming a canted C-type structure at $T_{N,B} = 78$ K; the A' -site Mn^{3+} ions also order AFM at lower temperatures $T_{N,A'} = 21$ K.¹¹ Here, we report on a record high electric polarization of $\sim 0.5 \mu\text{C cm}^{-2}$ in polycrystalline LMO samples induced by the magnetic order at $T_{N,B}$, and so even higher values promising for applications are expected in single-crystalline samples.

The LMO samples studied in the present work are 4 mm diameter cylinders synthesized under high-pressure as described elsewhere.¹¹ Depending on synthesis conditions, either powders or small, ≤ 0.5 mm-sized, single crystals are obtained. Powders are typically 95% pure and contain minor LaMnO_3 and Mn_3O_4 impurities. One powder sample was studied by x-ray diffraction as a function of temperature in a D8 Bruker diffractometer equipped with a focusing

primary Ge(111) monochromator for Cu $K_{\alpha 1}$ radiation and a close-cycle He cryostat. Pyrocurrent, I_p , measurements were carried out on three 0.2 mm thick disks of sintered powders of the same batch. The size of the available single crystals was too small for these measurements. Electrodes were realized by depositing a 0.1 μm thick Au layer on both sides of the disks by magnetron sputtering. The disks were cooled in a close-cycle cryogenic system down to $T_p = 100$ K, at which a poling field $E_p = 3\text{--}36$ kV cm^{-1} was applied for 30 min. At this temperature, the dc resistance of the samples exceeds 1 $\text{G}\Omega$, which ensures their full polarization. We subsequently cooled the samples down to 15 K, removed the poling field, and applied a short-circuit for 10 min to remove space charges. I_p was then measured upon warming-up the samples up to 150 K at rates of 2–5 K min^{-1} . On the same polycrystalline samples, we carried out complementary measurements of impedance, $Z(T, f)$, at frequencies, f , in the 1 kHz–1 MHz range, using a commercial LCR-meter combined with a Quantum Design Physical Property Measurement System (PPMS), and of field-dependent specific-heat, $C(T, H)$, using a 2τ relaxation method in zero-field cooling by ramping the field up to $H = 9$ T at constant temperature in the 2–60 K range.

Figure 1 shows the behavior of the unit cell parameters down to 9 K. No anomalous behavior is found for any of these parameters, except for the monoclinic angle, β , which displays a kink at $T_{N,B}$, consistent with previous powder neutron diffraction data.¹¹ This

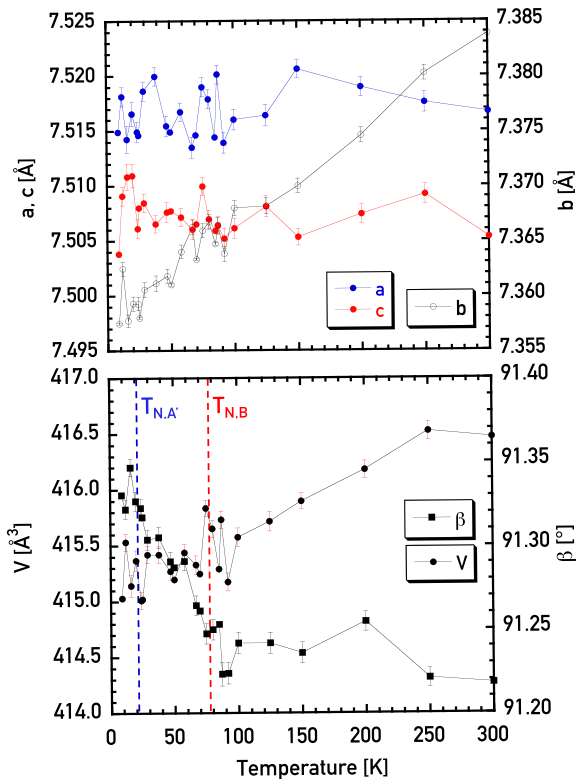


FIG. 1. Temperature dependence of the $I2/m$ unit cell parameters and volume, V , of $(\text{LaMn}_3)\text{Mn}_4\text{O}_{12}$ powders. Note the sudden increase in the β angle below the AFM ordering temperature of the B -sublattice, $T_{N,B}$, which indicates a large magnetoelastic coupling.

indicates a sizable magnetostriction along the diagonal of the ac -plane. In Fig. 2(a), the $I_p(T)$ results at different heating rates for both positive and negative E_p show that this distortion is concomitant with the appearance of ferroelectricity. The $I_p(T)$ curves reproducibly exhibit a pronounced peak near $T_{N,B}$, which changes sign according to the polarity of E_p , a signature of ferroelectricity induced by the ordering of the B -site Mn^{3+} ions. The shift of the I_p peak toward high temperatures with the increasing heating rate is due to a delay in sample thermalization, which explains the difference between the onset temperature of the peak and $T_{N,B}$.

Above 120 K, one observes a sudden increase in I_p , a characteristic signature of the leak current of thermally activated charges since the sign of this current does not change with the polarity of E_p . This explanation is consistent with the drop of sample resistance above this temperature, seen in the impedance curve, $Z(T)$, of Fig. 2(b). This

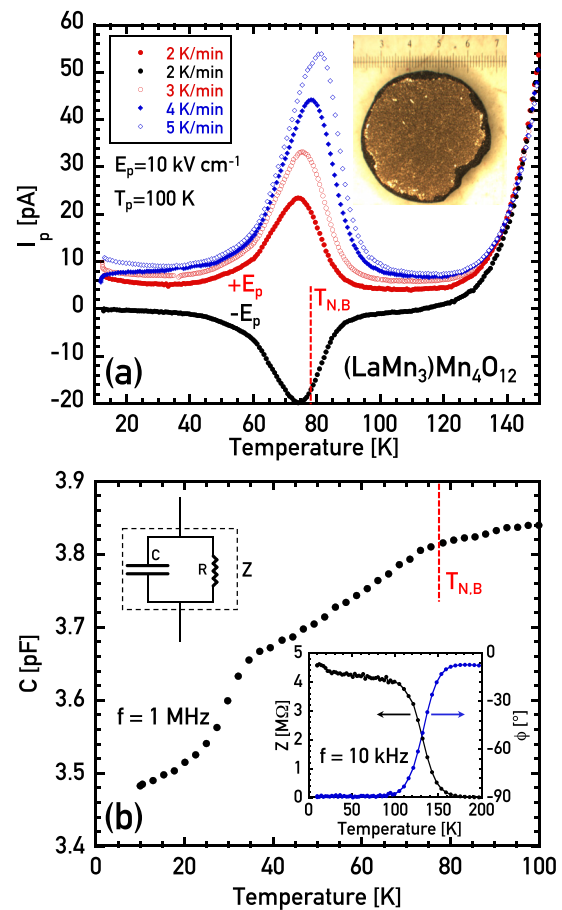


FIG. 2. (a) Pyrocurrent, I_p , measured on polycrystalline sample No. 1 at different heating rates (see legend) for positive and negative poling fields, $E_p = \pm 10$ kV cm^{-1} . T_p denotes the poling temperature. Note the peak near the AFM ordering at $T_{N,B} = 78$ K. Inset: the measured disk of LMO sintered powders covered by a Au layer. (b) temperature-dependence of the sample capacitance, C , extracted from the complex-impedance, Z and ϕ , data of the inset using a parallel RC equivalent circuit (see inset). f denotes the frequency of the measurements. The C -values are not converted into a dielectric constant owing to the uncertain contribution of the Schottky barrier created by the Au layer, as discussed in Ref. 14.

drop reflects the previously reported semiconducting behavior of LMO.¹¹ The dependence of the phase, $\phi(T)$, of Z confirms that, below $T_p = 100$ K, the response of the sample is predominantly capacitive, i.e., $\phi \approx -90^\circ$, thus supporting the reliability of the I_p measurements. The Z data are therefore described by a parallel RC equivalent circuit, which enables us to extract the sample capacitance, $C(T)$, shown in Fig. 2(b), where one notes a kink at $T_{N,B}$. This anomaly corroborates the scenario of ferroelectricity induced by magnetic order.¹³

Figure 3 shows the remnant polarization curve, $P(T)$, obtained by integrating the $I_p(T)$ curve of sample Nos. 1 and 2 for different poling fields, E_p . In the inset, a plot of the low-temperature (15 K) values of P with E_p shows the characteristic dependence expected for ferroelectrics: P first rapidly increases with E_p and then tends to level off at $0.45 \mu\text{C cm}^{-2}$ for the maximum value of the poling field used, $E_p = 36 \text{ kV cm}^{-1}$. At this value, saturation is not yet achieved. To give an

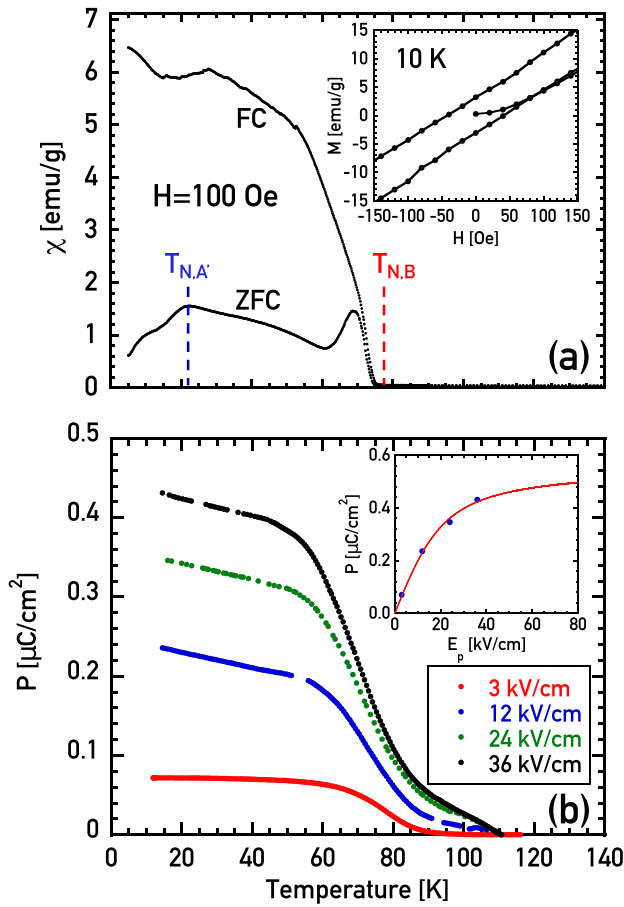


FIG. 3. (a) Magnetic susceptibility of a representative LMO single crystal measured at 100 Oe. Vertical broken lines indicate the AFM ordering temperatures, $T_{N,A'}$ and $T_{N,B}$, of the A' - and B -sublattices, respectively. Inset: details of the hysteresis behavior showing the weakly ferromagnetic response of the canted magnetic structure of LMO. (b): Remnant polarization, P , for different poling fields indicated in the legend and for a heating rate of 4 K/min. The curves are obtained by integrating the I_p curves of polycrystalline samples Nos. 1 (3 kV/cm data) and 2 (remaining data). Inset: dependence of P upon E_p . A fit of the experimental points using a Langevin function (red solid line) yields a saturation value $P_s = 0.56 \mu\text{C cm}^{-2}$.

estimate of the saturation value, P_s , we fit the data using a Langevin function and obtain $P_s = 0.56 \mu\text{C cm}^{-2}$. This value—which would not change significantly using alternative fitting functions—is a record for polycrystalline samples of magnetic ferroelectrics, twice as large as that previously reported on CMO single crystals.⁶ About 6–10 times larger values are expected in single crystalline film or bulk samples, as previously found in other manganese oxides displaying magnetic ferroelectricity.¹⁵ In CMO, for example, for poling fields of 4 kV cm^{-1} , P -values increase from $\approx 0.03 \mu\text{C cm}^{-2}$ in polycrystalline samples⁵ up to $0.28 \mu\text{C cm}^{-2}$ in single crystals.⁶

To explain the observation of magnetic ferroelectricity, we investigated the existence of a magnetoelastic (ME) coupling by measuring the effect of a magnetic field H on the specific heat, $C(T, H)$, at low-temperature. This coupling is expected to alter the phonon frequencies and thus the lattice contribution to C . This is confirmed in Fig. 4, where we report the H -dependence of $C(T, H)$ at constant temperature in field-cooling mode measured on the same batch of LMO powder samples. Note a dramatic reduction of C with the field, the relative reduction at 2 K being as large as 40% at 9 T. The reduction progressively decreases with temperature. Above 20 K, the contribution of the AFM transition $T_{N,A'} = 21$ K dominates over the magnetoelastic contribution.

We explain this result by Callen and Callen's theory¹⁶ of magnetoelastic coupling for cubic crystals, suitable for the present pseudocubic LMO system. The theory describes the magnetoelastic (ME) energy as an expansion of orthogonal modes for the strain field

$$H_{ME} = - \sum_{\mu} \sum_{j,l} B_{j,l}^{\mu} \sum_i \epsilon_i^{\mu,j} \mathfrak{R}_i^{\mu,l}, \quad (1)$$

where $B_{j,l}^{\mu}(T)$ are temperature-dependent magnetoelastic coefficients, j denotes the modes of a given irreducible representation Γ_{μ} (IR) of the strain coordinates $\epsilon_i^{\mu,j}$, i denotes the dimensions of the given IR, and $\mathfrak{R}_i^{\mu,l}$ are the cubic tensor operators (CTOs) of degree l forming an

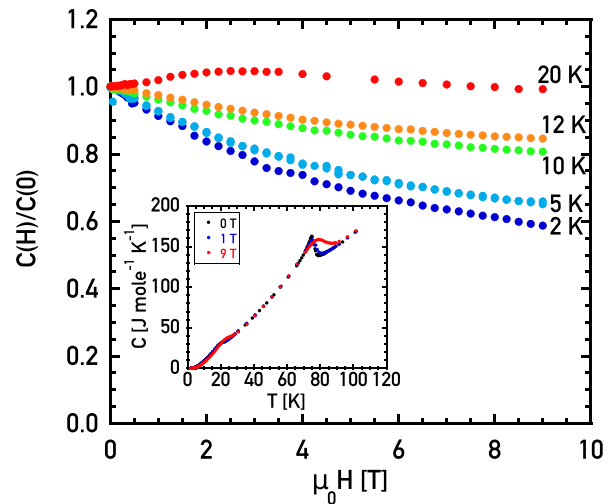


FIG. 4. Field-dependence of the specific heat, C , of a polycrystalline LMO sample at various temperatures. Inset: temperature dependence measured at different fields. Note the jumps at the AFM ordering temperatures, $T_{N,A'}$ and $T_{N,B}$, smeared by the field.

orthogonal basis. The Hamiltonian contains only even-degree CTOs, since the Hamiltonian is time-invariant. At low temperatures, the theory predicts that the $B_{j,l}^{\mu}(T)$ coefficients scale with the magnetization of the sublattice, consistent with the $l(l+1)/2$ power law originally established by Kittel and Van Vleck¹⁷

$$B_{j,l}^{\mu}(T)/\bar{B}_{j,l}^{\mu}(0) = [M(T)/M(0)]^{l(l+1)/2}. \quad (2)$$

By knowing the elastic constants of the compound, Eqs. (1) and (2) enable us to calculate all thermodynamic quantities like the specific heat of interest here. These constants are not available for LMO, and so we limit ourselves to analyze the power-law behavior of the $C(H)$ curve expected from Eq. (2). To do so, we consider the external strain caused by an external field, H , which corresponds to the $j=0$ strain coordinates for a given IR. The leading contribution is given by the lowest-order ($l=2$) mode present in the quadrupolar (E_g) Γ_7 IR, which is expected to give a characteristic $\sim M(T)^3$ dependence.¹⁶ Since the free energy depends quadratically on the ME coefficients, one finds that the corresponding ME contribution to the specific heat is described by a sum of two power-laws

$$\frac{C_{ME}}{T} \sim -\frac{\partial^2 (\bar{B}_{0,2}^{\gamma})^2}{\partial T^2} \sim \left[3M^5 \frac{\partial^2 M}{\partial T^2} + 7M^4 \left(\frac{\partial M}{\partial T} \right)^2 \right]. \quad (3)$$

Therefore, at a given temperature, the ME contribution C_{ME} grows rapidly with M following a combination of two power laws of indices 4 and 5, the weight of each depending on the slope and curvature of the $M(T)$ curve, respectively.

We apply the above considerations to LMO whose M vs H dependence exhibits a pronounced kink at $H^* \sim 0.1$ T [see Fig. 5(a) and Ref. 11]. Consistent with the hysteretic behavior of the magnetization in Fig. 3(a), this dependence is characteristic of canted AFM structures¹⁸ like the AFM C-type structure of LMO.¹¹ Namely, with the increasing field, the canting angle is gradually reduced until saturation of the canted component is achieved at H^* corresponding to $M^* \approx 52$ emu/g below 10 K. At higher fields, the response then becomes AFM-like, i.e., M increases linearly with H , as indeed observed in Fig. 5. The experimental M vs H dependence enables us to plot $C(H)$ as a function of M , which we did in Fig. 5(b) for the 2 K data. Interestingly, note a threshold behavior exactly at M^* above which the specific heat decreases rapidly, which gives evidence that the specific heat reduction scales with the magnetization. In addition, a simple data fit indicates that the M vs C behavior above M^* is well described by the sum of power laws of Eq. (3). An analysis of the magnitude of the C -reduction with M would require a measurement of the elastic constants, which goes beyond the scope of the present work.

The above finding of large ferroelectric polarization induced by a canted AFM structure and the evidence of a large magnetoelastic coupling raise a number of questions.

- (i) As in previously reported magnetic ferroelectrics like TbMnO_3 ,¹⁹ we have no indication of noncentrosymmetric distortions in LMO, as confirmed by recent high-resolution synchrotron x-ray diffraction study below $T_{N,B}$.²⁰ This discrepancy may be due to the difficulty in detecting these distortions by means of diffraction techniques. In alternative, we envisage the existence of polar domains in the nanometer-scale detected by microscopic and spectroscopic techniques, as reported recently on $(\text{Ca,Sr})_3\text{Ti}_2\text{O}_7$.²¹

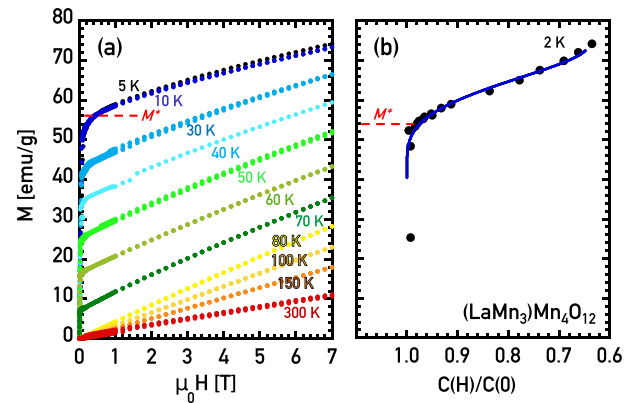


FIG. 5. (a) Magnetization, $M(H)$, curves measured at various temperatures on the same LMO single crystal of Fig. 3(a). (b) M -dependence of the 2 K $C(H)$ data of Fig. 4. The experimental points (black dots) are obtained using the 5 K $M(H)$ data of panel (a), unchanged below 10 K. The solid blue line is a best fit using Eq. (3). Note the same threshold behavior at M^* for both curves.

Therefore, a similar experimental study may be suitable to verify this scenario in LMO.

- (ii) As mentioned before, the magnetoelastic response of the β angle indicates that P should lie along the ac -diagonal, thus lowering the $I2/m$ symmetry to Im . Hence, considering that the magnetic structure displays AFM-coupled collinear moments in the ac -plane, the ferroelectricity should be driven by the symmetric exchange coupling. In the scenario of magnetic ferroelectricity proposed for collinear E-type magnetic structures like that of TbMnO_3 ,³ a polar distortion is driven by a competition between AFM and ferromagnetic (FM) superexchange interaction between neighboring Mn^{3+} ions. A similar scenario may apply here, for in LMO as well, the strong tilt of the MnO_6 octahedra characteristic of the QP structure, corresponding to a Mn-O-Mn bond angle $\approx 136^\circ$, does indeed lead to a strong competition, evident from the fact that, in the C-type structure of LMO, the interaction is AFM along the a - or c -direction and FM along the b -direction.¹¹ In the presence of this competition, the Im symmetry would therefore trigger the formation of non-equivalent pairs of neighboring Mn^{3+} ions within the ac -plane, thus leading to polar distortions.
- (iii) The large polarizations in CMO and LMO suggest that the $(\text{AMn}_3)\text{Mn}_4\text{O}_{12}$ system is favorable for hosting magnetic ferroelectricity. This may be explained by the fact that the aforementioned AFM-FM competition is maximized by the above tilt angle—remarkably constant in all quadruple perovskites—for this angle is intermediate between 90° and 180° . Further favorable conditions may be given by the following features of this structure:²² (1) the absence of oxygen defects; (2) the high $2/m$ symmetry of the oxygen sites (higher than in simple perovskites) hinders the distortions of the oxygen sublattice that would tend to screen the electric dipole.

In conclusion, we reported on ferroelectricity with a record large remnant polarization, $P_s = 0.56 \mu\text{C cm}^{-2}$, in polycrystalline samples of the quadruple perovskite LMO, concomitant with a canted AFM ordering of the B -site Mn^{3+} ions at $T_{N,B} = 78$ K, accompanied by sizable magnetostriction and magnetoelastic effects. The present finding is striking in two aspects: (i) the above values of polarization, twice as large as those found in CMO single

crystals, are obtained on polycrystalline samples, and so one expects values as high as $\sim 3\text{--}6 \mu\text{C cm}^{-2}$ —comparable to those obtained in proper ferroelectrics—in single crystalline LMO samples, which would be very promising for applications. (ii) If the picture of polarization in the *ac*-plane will be confirmed, the collinear properties of the AFM order in the *ac*-plane would support a scenario of ferroelectricity driven by a symmetric exchange coupling between Mn^{3+} ions, thus providing a clear guideline for the optimization of the multiferroic properties of magnetic ferroelectrics.

The authors acknowledge fruitful discussions with L. Chapon, M. Marezio, I. Mirebeau, and M. Mostovoy and financial support provided by the FAPESP Project Nos. 2012/21171-5, 2013/07296-2, 2013/27097-4 and 2017/24995-2, the CAPES-COFECUB Project No. Ph 878-17 (88887.130195/2017-01), and the Leonardo da Vinci program of the Université Franco-Italienne.

REFERENCES

- ¹W. Eerenstein, N. D. Mathur, and J. F. Scott, *Nature* **442**, 759 (2006).
- ²S.-W. Cheong and M. Mostovoy, *Nat. Mater.* **6**, 13 (2007).
- ³I. A. Sergienko, C. Şen, and E. Dagotto, *Phys. Rev. Lett.* **97**, 227204 (2006).
- ⁴T. Aoyama, K. Yamauchi, A. Iyama, S. Picozzi, K. Shimizu, and T. Kimura, *Nat. Commun.* **5**, 4927 (2014).
- ⁵G. Zhang, S. Dong, Z. Yan, Y. Guo, Q. Zhang, S. Yunoki, E. Dagotto, and J.-M. Liu, *Phys. Rev. B* **84**, 174413 (2011).
- ⁶R. D. Johnson, L. C. Chapon, D. D. Khalyavin, P. Manuel, P. G. Radaelli, and C. Martin, *Phys. Rev. Lett.* **108**, 067201 (2012).
- ⁷M. Marezio, P. Dernier, J. Chenavas, and J. Joubert, *J. Solid State Chem.* **6**, 16 (1973).
- ⁸X. Z. Lu, M.-H. Whangbo, S. Dong, X. G. Gong, and H. J. Xiang, *Phys. Rev. Lett.* **108**, 187204 (2012).
- ⁹J. T. Zhang, X. M. Lu, J. Zhou, H. Sun, F. Z. Huang, and J. S. Zhu, *Phys. Rev. B* **87**, 075127 (2013).
- ¹⁰R. D. Johnson, D. D. Khalyavin, P. Manuel, A. Bombardi, C. Martin, L. C. Chapon, and P. G. Radaelli, *Phys. Rev. B* **93**, 180403 (2016).
- ¹¹A. Prodi, E. Gilioli, R. Cabassi, F. Bolzoni, F. Licci, Q. Huang, J. W. Lynn, M. Affronte, A. Gauzzi, and M. Marezio, *Phys. Rev. B* **79**, 085105 (2009).
- ¹²H. Okamoto, M. Karppinen, H. Yamauchi, and H. Fjellvåg, *Solid State Sci.* **11**, 1211 (2009).
- ¹³Hysteresis loop *P*-*E* measurements were also carried out but the result was not conclusive because of the small signal-to-noise ratio. This is explained by the small sample capacitance $\sim 3\text{--}4$ pF to be measured, which reflects the comparatively small polarizations, as compared to proper ferroelectrics. Due to this experimental limitation, which is typical for magnetic ferroelectrics, pyroelectric current—instead of hysteresis—measurements have been widely employed to characterize these ferroelectrics. See, for example, the aforementioned case of CMO, ^{5,6} similar to ours.
- ¹⁴R. Cabassi, F. Bolzoni, A. Gauzzi, E. Gilioli, A. Prodi, and F. Licci, *Phys. Rev. B* **74**, 045212 (2006).
- ¹⁵S. Ishiwata, Y. Kaneko, Y. Tokunaga, Y. Taguchi, T.-H. Arima, and Y. Tokura, *Phys. Rev. B* **81**, 100411 (2010).
- ¹⁶E. R. Callen and H. B. Callen, *Phys. Rev.* **129**, 578 (1963).
- ¹⁷C. Kittel and J. H. Van Vleck, *Phys. Rev.* **118**, 1231 (1960).
- ¹⁸P. Wachter, L. Degiorgi, G. Wetzel, H. Schwer, K. Mattenberger, T. Herrmannsdorfer, and P. Fischer, *Acta Phys. Pol. A* **97**, 43 (2000).
- ¹⁹H. C. Walker, F. Fabrizi, L. Paolasini, F. de Bergevin, J. Herrero-Martin, A. T. Boothroyd, D. Prabhakaran, and D. F. McMorrow, *Science* **333**, 1273 (2011).
- ²⁰M. Verseils, A. J. Gualdi, B. Baptiste, P. Giura, C. Bellin, A. Polian, K. Béneut, M. D'Astuto, P. S. Pizani, A. J. A. De Oliveira, R. Cabassi, F. Bolzoni, E. Gilioli, M. B. Lepetit, R. Lobo, and A. Gauzzi (unpublished).
- ²¹M. H. Lee, C.-P. Chang, F.-T. Huang, G. Y. Guo, B. Gao, C. H. Chen, S.-W. Cheong, and M.-W. Chu, *Phys. Rev. Lett.* **119**, 157601 (2017).
- ²²A. Gauzzi, G. Rouse, F. Mezzadri, G. L. Calestani, G. André, F. Bourée, M. Calicchio, E. Gilioli, R. Cabassi, F. Bolzoni, A. Prodi, P. Bordet, and M. Marezio, *J. Appl. Phys.* **113**, 043920 (2013).